

ORIGINAL ARTICLE

Aqueous metabolome of tissue-specific conditional *Pten*-knockout mouse prostate cancer and TRAMP neuroendocrine carcinoma

Sangyub Kim PhD¹ | Li Li PhD² | Jinhui Zhang PhD² | Cheng Jiang MD^{1,2} | Junxuan Lü PhD^{1,2}

¹Department of Pharmacology, Pennsylvania State University College of Medicine, Hershey, Pennsylvania, USA

²Department of Biomedical Sciences, Texas Tech University Health Sciences Center, Amarillo, Texas, USA

Correspondence

Junxuan Lü, PhD, Department of Pharmacology, Pennsylvania State University College of Medicine, Hershey, PA 17033, USA.

Email: junxuanlu@pennstatehealth.psu.edu

Present address

Sangyub Kim, Zentalis Pharmaceuticals, San Diego, California, USA.

Li Li and Jinhui Zhang, Food and Drug Administration, Silver Spring, Maryland, USA.

Funding information

National Institutes of Health National Cancer Institute (NCI). Grant/Award Numbers: R01CA172169, R21CA218774

Abstract

Background: Metabolic reprogramming is now a recognized hallmark of cancer. The prostate-specific phosphatase and tensin homolog deleted on chromosome 10 (*Pten*) gene-conditional knockout (KO) mouse carcinogenesis model is highly desirable for studying prostate cancer biology and prevention due to its close resemblance of primary molecular defects and histopathological features of human prostate cancer. We have recently published macromolecular profiling of this model by proteomics and transcriptomics, denoting a preeminence of inflammation and myeloid suppressive immune cell features. Here, we performed metabolomic analyses of *Pten*-KO prostate versus wild type (WT) counterpart for discernable changes in the aqueous metabolites and contrasted to those in the TRAMP neuroendocrine carcinoma (NECa).

Methods: Three matched pairs of tissue-specific conditional *Pten*-KO mouse prostate and WT prostate of litter/cage-mates at 20–22 weeks of age and three pairs of TRAMP NECa versus WT (28–31 weeks) were profiled for their global aqueous metabolite changes, using hydrophilic interaction liquid chromatography-tandem mass spectrometry.

Results: The *Pten*-KO prostate increased purine nucleotide pools, cystathionine, and both reduced and oxidized glutathione (GSH, GSSG), and gluconate/glucuronate species in addition to cholesteryl sulfate and polyamine precursor ornithine. On the contrary, *Pten*-KO prostate contained diminished pools of glycolytic intermediates and phosphorylcholine derivatives, select amino acids, and their metabolites. Bioinformatic integration revealed a significant shunting of glucose away from glycolysis-citrate cycle and glycerol-lipid genesis to pentose phosphate cycle for NADPH/GSH/GSSG redox and pentose moieties for purine and pyrimidine nucleotides, and glycosylation/glucuronidation. Implicit arginine catabolism to ornithine was consistent with immunosuppression in *Pten*-KO model. While also

Sangyub Kim, Li Li, and Jinhui Zhang contributed equally to this study and they are co-first authors.

Preliminary results were communicated at the American Association for Cancer Research annual meeting in Washington, DC, April 2017 (Jinhui Zhang, Li Li, Sangyub Kim, et al., Integrative Analysis of Transcriptomic, Proteomic, and Metabolomic Data of *Pten*-Knockout Carcinogenic Mouse Prostate).

This is an open access article under the terms of the Creative Commons Attribution-NonCommercial License, which permits use, distribution and reproduction in any medium, provided the original work is properly cited and is not used for commercial purposes.

© 2021 The Authors. *The Prostate* published by Wiley Periodicals LLC

increased in cystathionine-GSH/GSSG, purine, and pyrimidine nucleotide pools and glucuronidation at the expense of glycolysis-citrate cycle, the TRAMP NECa increased abundance of many amino acids, methyl donor S-adenosyl-methionine, and intermediates for phospholipids without increasing cholesteryl sulfate or ornithine.

Conclusions: The aqueous metabolomic patterns in *Pten*-KO prostate and TRAMP NECa shared similarities in the greater pools of cystathionine, GSH/GSSG redox pair, and nucleotides and shunting away from glycolysis-citrate cycle in both models. Remarkable metabolic distinctions between them included metabolisms of many amino acids (protein synthesis; arginine-ornithine/immune suppression) and cholesteryl sulfate and methylation donor for epigenetic regulations.

KEYWORDS

adenocarcinoma, metabolic biomarkers, neuroendocrine carcinoma, prostate cancer

1 | INTRODUCTION

Activation of oncogenes and/or loss of tumor suppressor genes alter the metabolism of cancer cells to support their growth and survival.¹ Cancer metabolic reprogramming is now recognized as a hallmark of cancer.² The phosphatase and tensin homolog deleted on chromosome 10 gene (*PTEN*) loss is a frequent early pathogenetic change and a major oncogenic driver in human prostate cancer (PCa).³ The loss of *PTEN* alters its pivotal role in regulating various biological functions, including signal transductions, macromolecular alterations (engine), and metabolic reprogramming (fuels).^{4–6}

Metabolomic profiling allows an understanding of the global metabolic milieu changes associated with and perhaps even driving a particular cancer pathophysiology.⁷ The prostate-specific *Pten*-conditional knockout (KO) mouse carcinogenesis model is highly desirable for studies of prostate cancer biology and prevention due to its close resemblance of primary molecular defect and many histopathological features of human prostate cancer including androgen response, disease progression from prostatic intraepithelial neoplasia to adenocarcinoma, and a strong immunosuppressive tumor microenvironment (TME).^{8,9} We have recently published macromolecular profiling of this model by proteomics and transcriptomics¹⁰ and contrasted with TRAMP and c-Myc transgenic mouse models of prostate carcinogenesis. Based on macromolecular omics as well as literature reports of *Pten*/AKT-mTOR signaling, we implicitly presumed the hypothesis that *Pten*-KO prostate undergoes altered global metabolism conducive for carcinogenesis and that some of the metabolic changes may be specific when compared to a different model of prostate carcinogenesis by different onco-driver such as the TRAMP model. Here we examined the aqueous metabolite metabolomics of *Pten*-KO mutant prostate to profile and incorporate metabolic disturbances into the *Pten*-KO driven carcinogenesis process. We applied the same metabolomics platform to the TRAMP model and compared and contrasted between these two pathogenetic models.

2 | MATERIALS AND METHODS

2.1 | Source of biospecimens

As described in detail previously,¹⁰ the mouse tissues were provided by the Mouse Model Repository for Cancer Biomarker Discovery led by Christopher J. Kemp, PhD, at the Fred Hutchinson Cancer Research Center, sponsored by National Cancer Institute Mouse Proteomics Initiative (<http://proteomics.cancer.gov/programs/completed/mouseinitiave10>). Tissues were collected and cryopreserved from mice of *Pten*-KO genotype and their wild type (WT) litter-/cage-mates in 129 background from April 2005 to April 2007.

The frozen tissue specimens were shipped to Texas Tech University Health Sciences Center School of Pharmacy, Amarillo, on dry ice (received on August 2, 2011) and stored at -80°C until analyses. The litter-/cage-mate paired tissues allowed comparison of the genotypic differences with strict control of housing and environmental factors, breeding stock, and age variations among the *Pten*-KO and WT mice. For the *Pten*-KO and matched prostate specimens obtained from mice aged 20–22 weeks, we divided the frozen tissues into smaller portions and used the leftover portions from the mRNA microarray omics for the metabolomics. The extraction protocols for each omic were unique to its platform and had to be performed separately. As described in our previous paper,¹⁰ the proteomics analyses were carried out on a different batch of WT and KO matched pairs at the younger age of 12–15 weeks. Due to the frozen nature of tissues obtained from the National Cancer Institute (NCI) repository, histology was not available. However, the pathology was assumed to involve invasive adenocarcinoma based on published work of the originator laboratory of Hong Wu, PhD,⁸ with significant infiltration of myeloid-derived immune cells and inflammatory cells.⁹

By the same procurement procedure as the *Pten*-KO pairs, three pairs of frozen TRAMP tumor and WT prostate in litter-/cage-mates of 28, 29, and 31 weeks of age were also obtained. The matched pairs of mice were sacrificed on respective dates when a palpable pelvic

mass was detected in the transgenic sibling. Similarly, lack of histology information, the TRAMP tumors were presumed poorly differentiated neuroendocrine carcinomas (NECa) based on literature from groups of authoritative experimental/veterinary pathologists¹¹ and our own.¹² Due to the frozen nature of tissues as described above, we were not able to obtain specific lobes for the WT prostate of either model. We presume the prostate tissues sampled in our metabolomics work were mixture of different lobes.

2.2 | Tissue sample extract preparation

The frozen tissue samples were homogenized in 30 volumes (v/w) of precooled (-80°C) 80% methanol in water and stored at -80°C for 16 h. The homogenates were centrifuged at 14,000 g for 10 min in a refrigerated centrifuge at 4°C . The supernatants were saved at -80°C and analyzed by the following protocol.

2.3 | Metabolomics

The protocol published by Yuan et al.¹³ was adapted to profile aqueous endogenous metabolites from the tissue homogenate supernatants prepared in 80% methanol/water. The platform used hydrophilic interaction liquid chromatography with positive/negative ion switching to monitor 289 Q1/Q3 transitions from a single LC-MS/MS acquisition with a 5 ms dwell time and a 1.55 s cycle time. A UHPLC system (Nexera, Shimadzu) was coupled to a hybrid triple quadrupole linear ion trap mass spectrometer (QTRAP 5500, AB Sciex). Chromatographic separation was performed on an XBridge BEH Amide Column (hydrophilic interaction liquid chromatography, $100 \times 4.6 \times 3.5 \mu\text{m}$, Waters). The column oven temperature was kept at 40°C .

To ensure sensitive detection within the linear dynamic range, each extract was analyzed by multiple UHPLC-MS/MS runs with the injection volume of 10 and $1 \mu\text{l}$. The abundance of each endogenous metabolite varied over a wide range, some of them were not able to be detected when $1 \mu\text{l}$ extract was injected; whereas the signal of some metabolites was saturated when $10 \mu\text{l}$ extract was injected. For $1 \mu\text{l}$ volume injections, all were done in duplicate. For $10 \mu\text{l}$ volume injections, most was done in duplicates, some in triplicates. The identification of metabolites was performed as per the Yuan report.¹³

2.4 | Data curation and statistical metrics

The average/mean of the replicate measurements (peak area) was calculated and used for computation of the paired ratio (indicative of relative abundance) of each LC-MS/MS verified metabolite between *Pten*-KO or TRAMP prostate tumor and respective WT litter-/cage-mate. One-tailed, paired *t* test was administered on the peak areas in matched pairs (null hypothesis difference of tumor and WT pairs = 0) or on log-transformed peak area (null hypothesis ratio = 1 or

$\log(\text{Tumor}/\log\text{WT}) = 0$). Given the small number of pairs and inherent large variance among individual mice for metabolite analyses, $p \leq 0.1$ or one-tail log paired $p \leq 0.1$ was used as statistical threshold for differential abundance for metabolites between tumor and WT litter-/cage-mate samples and for inclusion in enrichment analyses. For exception in the *Pten*-KO model, nine metabolites of clinical relevance and with the ratio changes for all three pairs concordant in direction were included for analyses.

2.5 | Bioinformatic and metabolic enrichment analyses

We performed the statistical analysis and the enrichment analysis utilizing MetaboAnalyst 4.0 (link: www.metaboanalyst.ca/).¹⁴ The partial least-squares discriminant analysis (PLS-DA) model was used to highlight differences between *Pten*-KO or TRAMP tumors versus respective WT mouse prostate. For the creation of the heat maps, the selected metabolites were also hierarchically clustered by distance measure using Pearson's correlation and clustering algorithm using average linkage (clustering uses the centroids of the observations). The values were scaled metabolite-wise in columns for heatmap visualization. For the metabolic enrichment analyses, location-based metabolite sets and pathway-associated metabolite sets in MetaboAnalyst's enrichment analysis (MSEA) module were selected as a metabolite library for MSEA. The metabolic pathway map of the selected differential metabolites and significantly changed metabolic pathways was analyzed and visualized by iPath 3.0 software (<https://pathways.embl.de/ipath3.cgi>).

3 | RESULTS

3.1 | Aqueous metabolome of *Pten*-KO prostate

Using the UHPLC-MS/MS platform, we identified 177 endogenous metabolites in the mouse prostate aqueous extracts (Table S1, Raw data). With the exception of a detectable increase of cholesteryl sulfate, it was apparent for a lack of detection of hydrophobic lipids, fatty acids, cholesterol, and cholesteryl fatty acid esters. Table 1 summarized 44 selected metabolites (20 greater and 24 less in *Pten*-KO prostate than in WT prostate) that met criteria of statistical threshold or concordance of change directions described in Section 2 (more details in Table S1, select metabolites). A supervised PLS-DA of the variance of these select metabolites between the two genotypes showed an obvious separation of WT prostate tissue (green crosses) and *Pten*-KO mutant prostate (red triangles) (Figure 1A). The heatmap of the top 25 metabolites (14 more abundant, 11 less abundant than WT) (Figure 1B) showed distinctive clustering of the metabolites between the genotypes.

Some metabolites were remarkably increased in the *Pten*-KO prostate tumors (Table 1). They included many ribosyl- and deoxyribosyl nucleotides (ADP, ATP, IDP, dAMP, dCMP, dGDP, dGTP),

TABLE 1 Selected metabolites increased or decreased in *Pten*-KO versus WT prostate and comparison to TRAMP model and published data

Metabolite	Pten-KO/WT ratio (n = 3)		Pten-KO/ WT ^a	TRAMP/WT ratio (n = 3)		Human PCa ¹⁸	Human PCa ¹⁷
	Mean	SD		Mean	SD		
Increased in <i>Pten</i>-KO	Mean	SD		Mean	SD		
ADP	7.06	9.00	2.85	2.11	1.43		
ATP	17.04	25.33		1.64	0.74		
IDP	7.83	10.46	1.93	1.62	0.46		
dAMP	1.95	0.88		4.68	1.71		
dCMP	2.19	0.60		Missing data			
dGDP	7.58	9.95		1.59	0.64		
dGTP	20.80	31.91		1.73	0.78		
Uric acid	4.77	3.23	1.34	0.74	0.59	0.8	0.95
Aminoimidazole carboxamide ribonucleotide	1.29	0.20		Missing data			
Cytosine	1.53	0.25		0.05	0.01		
Cholesteryl sulfate	4.51	1.64	1.19	0.35	0.21		
Cystathionine	10.11	11.67		8.04	1.94		
Glutathione (GSH)	1.55	0.61	0.68	1.72	0.41		1.14
Glutathione disulfide (GSSG)	2.26	1.13		2.50	0.93		0.96
NADP ⁺	5.83	4.81	0.38	1.07	1.12	5.1	
Ornithine	3.75	2.47		2.50	1.76		1.42
Pantothenate	1.48	0.39		0.36	0.24		
p-Hydroxy-benzoate	1.52	0.18		1.01	0.10		
D-gluconate	1.50	0.18		1.12	0.36		
UDP-D-glucuronate	5.03	5.39		2.22	0.70		
Decreased in <i>Pten</i>-KO	Mean	SD		Mean	SD		
4-Amino-butyrate	0.22	0.16		1.95	1.78		1.00
N-Acetyl-glucos-amine	0.15	0.07	0.40	0.11	0.13	2.5	
N-Acetyl-L-alanine	0.44	0.24	2.41	0.58	0.28		
N-Acetyl-glutamate	0.47	0.06		Missing data		0.4	
Adenosine	0.39	0.28	0.28	0.16	0.15	0.6	0.91
Acadesine	0.32	0.23		1.63	0.35		
Guanine	0.55	0.34		1.24	0.47		
Creatinine	0.18	0.08	0.66	0.21	0.21		0.99
Creatine	0.62	0.19		0.77	0.12		
Dephospho-CoA	0.43	0.28		Missing data			
Dihydroxy-acetone- phosphate	0.26	0.11		0.33	0.13		
Glycerate	0.22	0.10	1.48	0.23	0.02		1.04

(Continues)

TABLE 1 (Continued)

Metabolite	Pten-KO/WT ratio (n = 3)		Pten-KO/WT ^a	TRAMP/WT ratio (n = 3)		Human PCa ¹⁸	Human PCa ¹⁷
Glycerophospho-choline	0.58	0.32		0.37	0.09		
Phosphoryl-choline	0.24	0.08	0.23	0.36	0.14		
Hydroxyphenyl-pyruvate	0.32	0.13	1.60	Missing data			
Myo-Inositol	0.66	0.32		0.39	0.16		
Nicotinamide- ribotide	0.55	0.26		0.38	0.09		
Oxaloacetate	0.86	0.06		0.61	0.04		
Sarcosine	0.61	0.30		0.96	0.30		
sn-Glycerol-3-phosphate	0.46	0.13	0.32	0.41	0.16	3	1.59
S-Ribosyl-L-homocysteine	0.27	0.16		0.09	0.11		
Trehalose-6-Phosphate	0.47	0.45		1.41	0.15		
Trehalose	0.50	0.06		1.02	0.11		

Note: Boldface metabolites and their fold ratio values met one or both *p*-value threshold.

^aZabala-Letona.¹⁶ We selected average 6-month data to compare with our data.

cytosine and nucleotide derivatives (AICA-ribonucleotide, NADP+, UDP-D-glucuronate), uric acid (a purine metabolite), glutathione (GSH) and its oxidized disulfide (GSSG) and key cysteine precursor cystathionine. Beside the increased abundance of cholesteryl sulfate, *Pten*-KO prostate contained a much-elevated level of ornithine, a known precursor to polyamines and a product of arginase to catalyze the release of urea from arginine (urea cycle).

On the other hand, metabolites with diminished abundance in the *Pten*-KO prostate (Table 1) included amino acid derivatives (N-acetyl-L-alanine, N-acetyl-glutamate, acetyl-lysine, S-ribosyl-L-homocysteine), purine base or nucleoside (adenosine, guanine), glycolysis intermediates, phosphorylcholine intermediates as well as other arginine and glycine metabolites such as creatine, creatinine, and sarcosine.

3.2 | Bioinformatic analyses of *Pten*-KO prostate metabolome data set and integration with key proteomic and transcriptomic changes

We used MESA to identify possible pathways and biologically meaningful patterns enriched in the metabolomic data (Tables 2 and S2). The functional enrichment analysis yielded nine significant metabolic pathways (two upregulated and seven downregulated pathways) with *p* < 0.05 (Table 2). *Purine metabolism* and *glutathione metabolism* were the two upregulated pathways. The seven downregulated pathways were *glycerophospholipid metabolism*; *arginine and proline metabolism*; *glycine, serine, and threonine metabolism*; *alanine, aspartate, and glutamate metabolism*; *glycerolipid metabolism*,

glycolysis, or gluconeogenesis; and *pyruvate metabolism*. Location-based metabolite sets MESA predicted that these metabolic pathways were mainly associated with mitochondria, lysosome, and prostate (Figure 1C). Not surprisingly, mitochondria and, to a less extent, lysosomes are the major subcellular organelles for providing building blocks as well as regulators of metabolic flux and redox activity in the cell.¹⁵

Based on mammalian biochemical reactions, Figure 2 mapped the majority of detected metabolite changes (bold for increased in *Pten*-KO; shaded white for decreased in *Pten*-KO) within the interconnected metabolic pathways, shunts, and cycles, focusing on glucose fates, GSH/GSSG, and their constituent amino acids glutamate, cysteine and glycine, and arginine/ornithine/urea cycle. The *Pten*-KO prostate shunted glucose away from glycolysis, as indicated by decreased dihydroxy-acetone-phosphate and glycerate and decreased glycerol/choline pool (decreased glycerol-3-phosphate, glycerophosphocholine, and phosphorylcholine), and from the flux through the citrate cycle, as indicated by diminished supply of acetyl-CoA to the mitochondria (decreased dephospho-CoA, and decreased acetylation of glutamate and select amino acids and glucosamine) and a modest decrease of oxaloacetate. Instead, glucose was channeled toward pentose phosphate cycle (increased gluconate) for NADPH production and for the pentose moieties essential for anabolic synthesis or salvage of purine and pyrimidine nucleotides for nucleic acids crucial cell proliferation; and to the glucuronidation pathway for Phase II drug metabolism (increased UDP-glucuronate). The *Pten*-KO prostate increased the overall synthesis of GSH and redox fluxes of GSH/GSSG pair. Increased cystathionine would fuel a steady supply of cysteine for GSH synthesis. Another key amino acid glycine for GSH

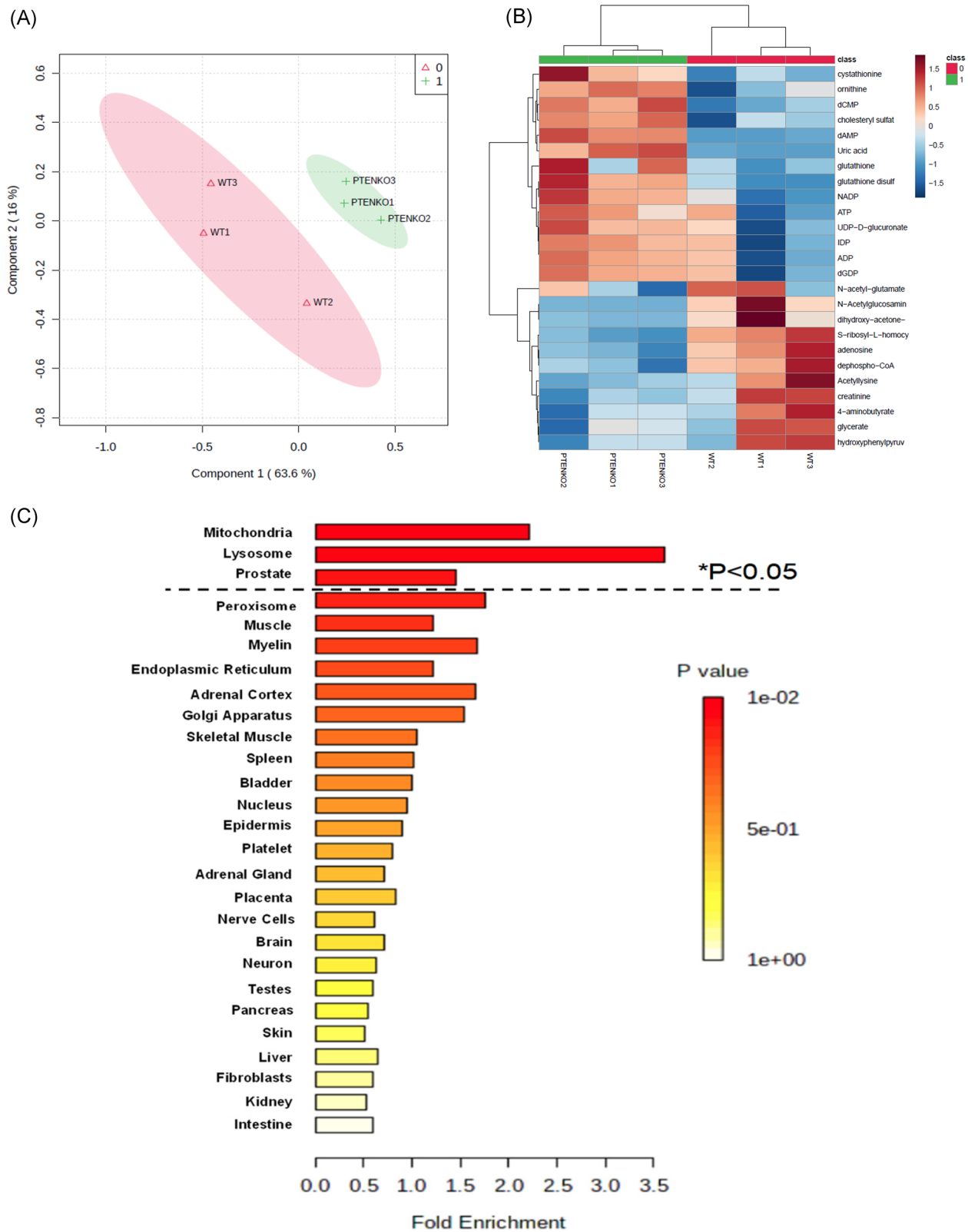


FIGURE 1 Metabolomic analyses of *Pten*-KO mouse prostate tumor model using MetaboAnalyst 4.0. (A) Metabolic profile of *Pten*-KO and wild type (WT) mouse prostates visualized by supervised partial least-squares discriminant analysis (PLS-DA) clustered by the samples with the three biological replicates of WT (red triangle) and three biological replicates of *Pten*-KO (green cross). (B) Heatmap for relative abundances of top 25 metabolites in litter-/cage-mates of WT and *Pten*-KO mice (i.e., WT1 vs. Pten1, WT2 vs. Pten2, and WT3 vs. Pten3). Columns represent each biological replicate, and rows represent individual metabolites. The more abundant metabolites in *Pten*-KO appeared red, and the less metabolites were colored in blue. (C) Location-based metabolite sets enrichment analysis (MSEA). The dashed lines indicate the cutoff *p* value ($*p < 0.05$). The color of the scale bar represents the *p* value [Color figure can be viewed at wileyonlinelibrary.com]

synthesis was likely made more available by diversion away from its S-adenosyl-methionine-driven methylation to generate sarcosine and the production of creatine via arginine:glycine aminotransferase (AGAT). For GSH/GSSG redox and GSH driven functions, we have reported increased protein abundance of glutathione disulfide reductase (GSR), glutathione S-transferases omega-1 (GSTO1) and A4 (GSTA4) and mRNA increases of *Gsto1*, glutathione peroxidase 2 gene (*Gpx2*), and hexose-6-phosphate dehydrogenase (*H6pd*) in the *Pten*-KO prostate.¹⁰

In addition to diversion from creatine/creatinine production, arginine was likely shunted away from nitric oxide synthesis (T cell maturation) to allow arginase to produce the polyamine precursor ornithine (part of the urea cycle). The mRNA level for *Arg1* (arginase 1) gene was much increased in our macromolecular omics analyses of *Pten*-KO prostate,¹⁰ consistent with and supportive of infiltration of myeloid-derived (immune) suppressive cells (MDSC) and inflammatory cells.⁹ Unfortunately, our metabolomics platform failed to detect any polyamines or their further metabolites (no detection in Table S1).

3.3 | Comparison with reported metabolomics datasets, and human relevance

As a measure of cross validation, we compared our data set with the metabolomics analysis reported by Zabala-Letona et al. of *Pten*-KO mouse prostate.¹⁶ They reported that the most prominently increased metabolites were higher-order polyamines, such as *N*-acetyl-spermidine and *N*-acetyl-spermine, which were not detected by our platform (Table S1). Four metabolites (IDP, ADP, uric acid, and cholesteryl sulfate) matched our panel of 20 increased metabolites (Table 1). In contrast to our finding of elevated abundance of NADP+ and glutathione (GSH), they reported decreased levels of both metabolites in the *Pten*-KO prostate tumors. Among the 24 decreased metabolites, they reported five that matched the same change trajectory, that is, *N*-acetylglucosamine, creatinine, phosphorylcholine, adenosine, and sn-glycerol-3-phosphate (Table 1). However, they reported increased levels of glycerate, hydroxyphenylpyruvate, and *N*-acetyl-L-alanine in the *Pten*-KO prostate. These discrepancies could be caused by the difference in the mass spectrometer type (QTRAP 5500 mass spectrometer (ours) vs. Agilent 6520 QToF mass spectrometer¹⁶), as well as the prostate tissue sample acquisition and extract preparation methods.

Regarding reported metabolite changes in human PCa specimens, NADP+, ornithine, glutathione, adenosine, and *N*-acetylglutamate were found to change in the same directions as in our *Pten*-KO mouse data set (Table 1). On the other hand, uric acid, GSSG, *N*-acetylglucosamine, glycerate, and sn-glycerol-3-phosphate did not change in the same patterns between human PCa and our profiled mouse *Pten*-KO prostate (Table 1). In particular, both the human PCa datasets from Jung et al.¹⁷ and Ren et al.¹⁸ could not detect ATP and most of other high-energy phosphorylated nucleotides (e.g., dGTP, dGDP, IDP, ADP, etc.). Previously, many studies

failed to show the consistent extraction of high-energy phosphorylated compounds (e.g., ATP and NADPH) known to be susceptible to degradation.¹⁹ A mixture of acetonitrile:methanol:water (40:40:20) with 0.1 M formic acid and subsequent neutralization with ammonium bicarbonate was considered as an effective solvent system for both quenching and extraction.¹⁹ The solvent systems used for their metabolite extractions (Ren paper: formic acid, ammonium bicarbonate, and methyl *tert*-butyl ether¹⁸; Jung paper: water/ethanol/dichloromethane/acetonitrile¹⁷) could be suboptimal for high-energy compounds.

3.4 | Aqueous metabolome of TRAMP NECa and comparison with *Pten*-KO prostate

In the TRAMP NECa, our aqueous metabolomics platform detected increased levels of cystathionine, GSH and GSSG, and purine and pyrimidine nucleotides of both ribose and deoxyribose, yet without a significant change of ornithine and even a decrease of cholesteryl sulfate over their paired counterpart WT prostate (Tables 1 and S3). We detected decreased levels in the TRAMP NECa of adenosine, creatine and creatinine, *N*-acetylglucosamine, glycerate, phosphorylcholine (PC), and glycerophosphocholine (GPC), as in the *Pten*-KO prostate. These concordant changes in both the *Pten*-KO and the TRAMP mouse prostate cancer models suggested that these metabolites could play common roles in prostate carcinogenesis, or the changes could be an indication of the disruption of normal prostate metabolic functions. An earlier study using (1)H-NMR showed that in TRAMP mice of 28 weeks of age, reduced tumor levels of citrate (49%), choline (33%), PC (57%), GPC (66%), and glycerophosphoinositol (61%) were observed relative to age-matched WT prostate ($p < 0.05$).²⁰

However, in contrast to the *Pten*-KO prostate, prominent increases of many amino acids and their metabolites were detected in the TRAMP NECa (Table S3). Indeed, pathway enrichment analyses (Table S4) showed that five of six significantly ($p < 0.05$) upregulated metabolic pathways were related to the metabolisms of *methionine*; *glycine and serine*; *homocysteine degradation*; *aspartate*; and *glutamate*. The other was *purine metabolism*.

Figure 3A showed a clear separation of the malignant TRAMP NECa from the WT prostate specimens by supervised PLS-DA of the variance of the differential metabolites between TRAMP (red triangles) and paired WT mouse prostate tissue (green crosses). The heatmap of the top 25 differential metabolites (18 more abundant, seven less abundant than WT) (Figure 3B) showed distinctive clustering of the metabolites between NECa and the normal prostate. Location-based metabolite sets MESA predicted that the altered TRAMP metabolic pathways were mainly associated with peroxisome and lysosome subcellular organelles and the implicated organs were related to NE signaling and innervations (*nerve cells*; *neuron*; *brain*; *prostate*, *pancreas*, *heart*, and *muscles*) (Figure 3C).

Figure 4 mapped the majority of detected metabolite changes (bold for increased in TRAMP NECa; shaded white for decreased in

TABLE 2 Altered metabolic Pathways in *Pten*-KO prostate identified using MetaboAnalyst 4.0 (selected if $p < 0.05$ for the metabolic network analysis)

Metabolism pathway	Direction of change	p value	Total	Hits	Selected metabolites altered in the pathway
Purine metabolism	Up	3.02E-07	92	8	AICA-riboside, ATP, ADP, dAMP, IDP, uric acid, dGDP, dGTP
Glutathione metabolism	Up	2.18E-04	38	4	Glutathione, oxidized glutathione, NADP, ornithine
Glycerophospholipid metabolism	Down	6.94E-04	39	4	Glycerol 3-phosphate, dihydroxyacetone phosphate, phosphorylcholine, glycerophosphocholine
Arginine and proline metabolism	Down	0.00117	77	5	N-Acetyl-L-alanine, creatine, creatinine, gamma-aminobutyric acid, sarcosine
Glycine, serine and threonine metabolism	Down	0.00154	48	4	Glycerate, dimethylglycine, sarcosine, creatine
Alanine, aspartate and glutamate metabolism	Down	0.00198	24	3	L-Alanine, gamma-aminobutyric acid, oxalacetic acid
Glycerolipid metabolism	Down	0.00457	32	3	Glycerol 3-phosphate, glycerate, dihydroxyacetone phosphate
Glycolysis or Gluconeogenesis	Down	0.0435	31	2	Oxalacetic acid, dihydroxyacetone phosphate
Pyruvate metabolism	Down	0.0461	32	2	Oxalacetic acid, dihydroxyacetone phosphate

Note: The bold face highlights a metabolite met statistical significance threshold for different between genotypes. Plain face showed change concordant in the direction (i.e., either all increased or all decreased) for all three pairs. These "exception" were included due to their clinical relevance, as noted in text.

TRAMP NECa) within the interconnected metabolic pathways, shunts, and cycles. TRAMP NECa appeared to shunt glucose away from glycolysis and citrate cycle, even more so than the *Pten*-KO prostate. Instead, glucose was channeled toward the glycosylation (increased UDP-glucose) and glucuronidation (increased UDP-glucuronate) pathways. As in the *Pten*-KO prostate, the TRAMP NECa increased GSH and GSSG, in association with increased cystathionine to increase cysteine, and shunting glycine away from degradation (i.e., decreased creatine and creatinine). Several distinctions from *Pten*-KO prostate were noteworthy. Foremost, the elevated pools of many amino acids would undoubtedly provide ample substrates for protein synthesis. Besides supporting protein synthesis, the extraordinarily elevated aspartate (Asp) and asparagine (Asn) and elevated carbamoyl-Asp might fuel the de novo syntheses of uracil and subsequent conversion to uridine, cytidine, and the further downstream ribosyl and deoxyribosyl pyrimidine nucleotides for RNA and DNA syntheses. In addition, the increased S-adenosyl-methionine (as well as its de-methylated product S-adenosyl-homocysteine) was interpreted as providing abundant methyl donor for the methylation epigenetic regulations of DNA and other macromolecules. An earlier study had shown DNA hypermethylation of poorly differentiated TRAMP tumors.²¹ Furthermore, in the TRAMP NECa, elevated levels of UDP-ethanolamine and UDP-choline plus depleted levels of ethanolamine and choline and choline phospho intermediary metabolites might be consistent with potential de novo synthesis of phosphatidyl lipids required for cell membranes in the malignant cells. Moreover, TRAMP NECa decreased arginine degradation (urea level) and did not increase ornithine production, nor uric acid but increased a purine degradation product allantoin which fell further downstream of uric acid.

4 | DISCUSSION

As PTEN deficiency leads to AKT-mammalian target of rapamycin (mTOR) activation in prostate driving proliferation and transformation of epithelial lesions,²² it was not surprising that increased *purine/nucleotides metabolism* became the most prominent feature in our aqueous metabolome outcome for *Pten*-KO prostate (Tables 1 and 2). The metabolisms of purine and pyrimidine are crucial to support the synthesis of nucleic acids.^{23,24} Purine synthesis has been reported to be modulated by mTORC1 downstream of the PI3K/PTEN/AKT pathway or vice versa.^{24,25} Similarly, *Pten* loss in mouse embryonic fibroblast (MEF) cells leads to glutamine to cascade through the de novo pyrimidine synthesis.²⁶ The faster-growing transformed cells in the *Pten*-KO prostate have a high demand for nucleotides for intensive synthesis of DNA and RNA. The transcriptomic profiling indicated greater expression of many transporters, likely enabling the greater fluxes of these needed nucleotides. The second prominent feature was increased *glutathione metabolism* in the *Pten*-KO prostate (Table 2; Figure 2). Elevated glutathione and its metabolisms are associated with a proliferative response and tumor progression in various types of tumors.²⁷ Serum cystathionine was higher in prostate cancer patients who developed rapid biochemical recurrence compared to age-matched recurrence-free patients.²⁸ Glutathione is an antioxidant that functions as a free radical scavenger by detoxifying hydrogen peroxide and lipid peroxides through GPXs, and we have reported the specific elevation of *Gpx2* mRNA in the *Pten*-KO prostate in microarray transcriptomics.¹⁰ Glutathione is synthesized from glutamate, cysteine, and glycine (Figure 2). In our network analysis, the metabolites in *glutathione metabolism* were increased (i.e., GSH and GSSG as well as cystathionine, which converted to key

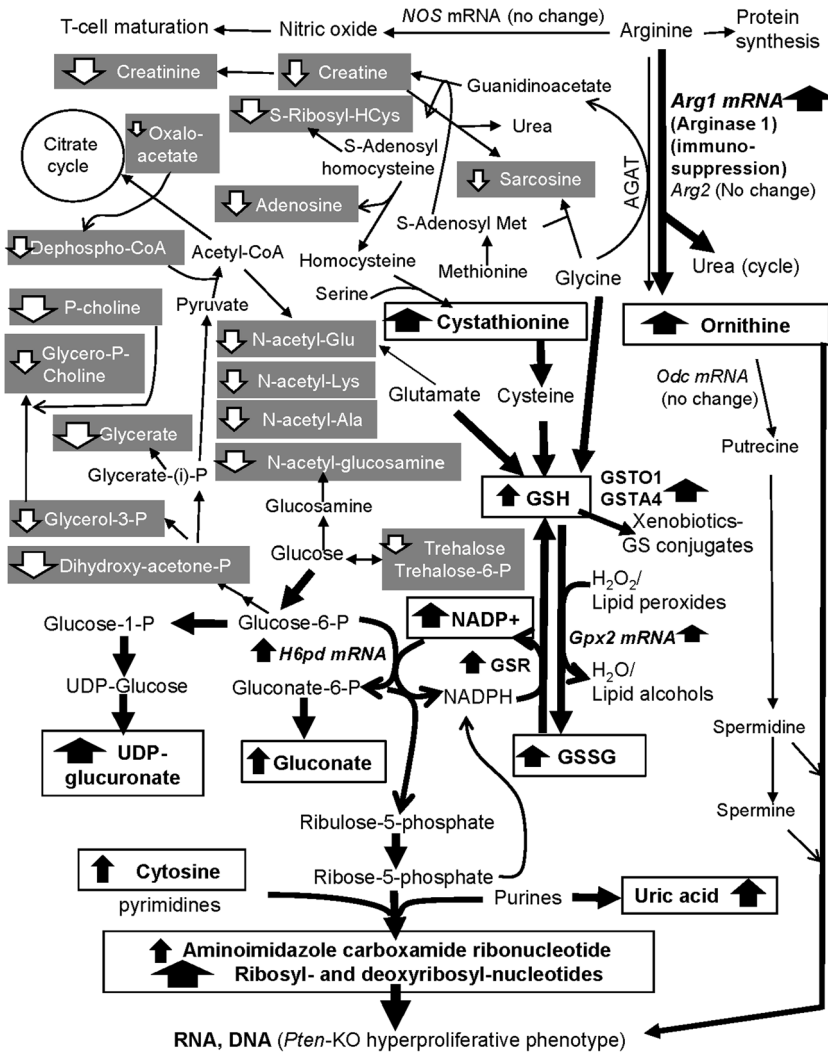


FIGURE 2 An integrated metabolic map of detected changes of metabolites in *Pten*-KO/wild type (WT) prostate focusing on glucose fates, glutathione and its constituent amino acids glutamate, cysteine and glycine, and arginine/ornithine urea cycle. Bold font in boxes indicates an increased metabolite in *Pten*-KO prostate; shaded white font indicates a decreased metabolite in *Pten*-KO prostate

amino acid cysteine for GSH synthesis), while those in *glycine, serine, and threonine metabolism* and *alanine, aspartate, and glutamate metabolism* were decreased in the *PTEN*-KO mutant prostate (Table 2; Figure 2), consistent with a tenet that these building blocks of glutathione were shunted toward more synthesis.²⁷ Important for the synthesis of glutathione, the trans-sulfuration pathway is involved in providing sulfur from methionine through cystathionine and eventually to cysteine.^{29,30} Consistent with our finding, GSSG in *Pten*-null mouse liver was found increased by twofold.³¹ The elevated glutathione metabolism in conjunction with increased expression of enzymes using GSH as a substrate (GSTO1, GSTA4 proteomics, *Gpx2* mRNA by microarray)¹⁰ might reflect greater redox flux and cytoprotection permissive for a tumor cell growth advantage.^{18,31} These two metabolic upregulation changes observed in the *Pten*-KO prostate were also observed in the TRAMP NECa, consistent with enhanced redox protection for proliferation of the malignant cells which required ample provision of purine and pyrimidine nucleoside/nucleotide substrates for their DNA and RNA syntheses.

Metabolisms of amino acids manifested a major distinction point between *Pten*-KO and TRAMP carcinogenesis. Arginine is a highly versatile amino acid and is associated with several biological

processes beside synthesis of proteins, including nitric oxide (NO) and T cell activation/maturation. As a key arginine catabolism product and polyamine precursor, ornithine was significantly increased in human prostate cancer tissues from radical prostatectomy compared to normal adjacent tissue.¹⁷ Ornithine is a key component of the urea cycle and it shuttles between the cytosol and mitochondria. Arginase-1 enzyme in the cytosol converts arginine to urea and ornithine, which can be decarboxylated to generate putrescine and subsequently to higher polyamines. The reshunting of arginine metabolism in the *Pten*-KO prostate was indicated by elevated abundance of ornithine and a decreased production of creatine and its dehydration product creatinine (Figure 2; Table 2) as a likely result of decreased arginine:glycine aminotransferase flux. Microarray transcriptomic analyses detected increase *Arg1* mRNA level, without change of *Arg2* or *Odc* mRNA.¹⁰ The increased *Arg1* mRNA expression and increased ornithine level in the *Pten*-KO prostate were consistent with the increased infiltrating MDSC cells in this model for an immune-suppressive TME as detailed by Hong Wu group⁹ and confirmed by our macromolecular omics.¹⁰ In contrast to no change or generally decreased amino acid levels in the *Pten*-KO prostate, the TRAMP NECa contained elevated pools of many amino acids and lacked

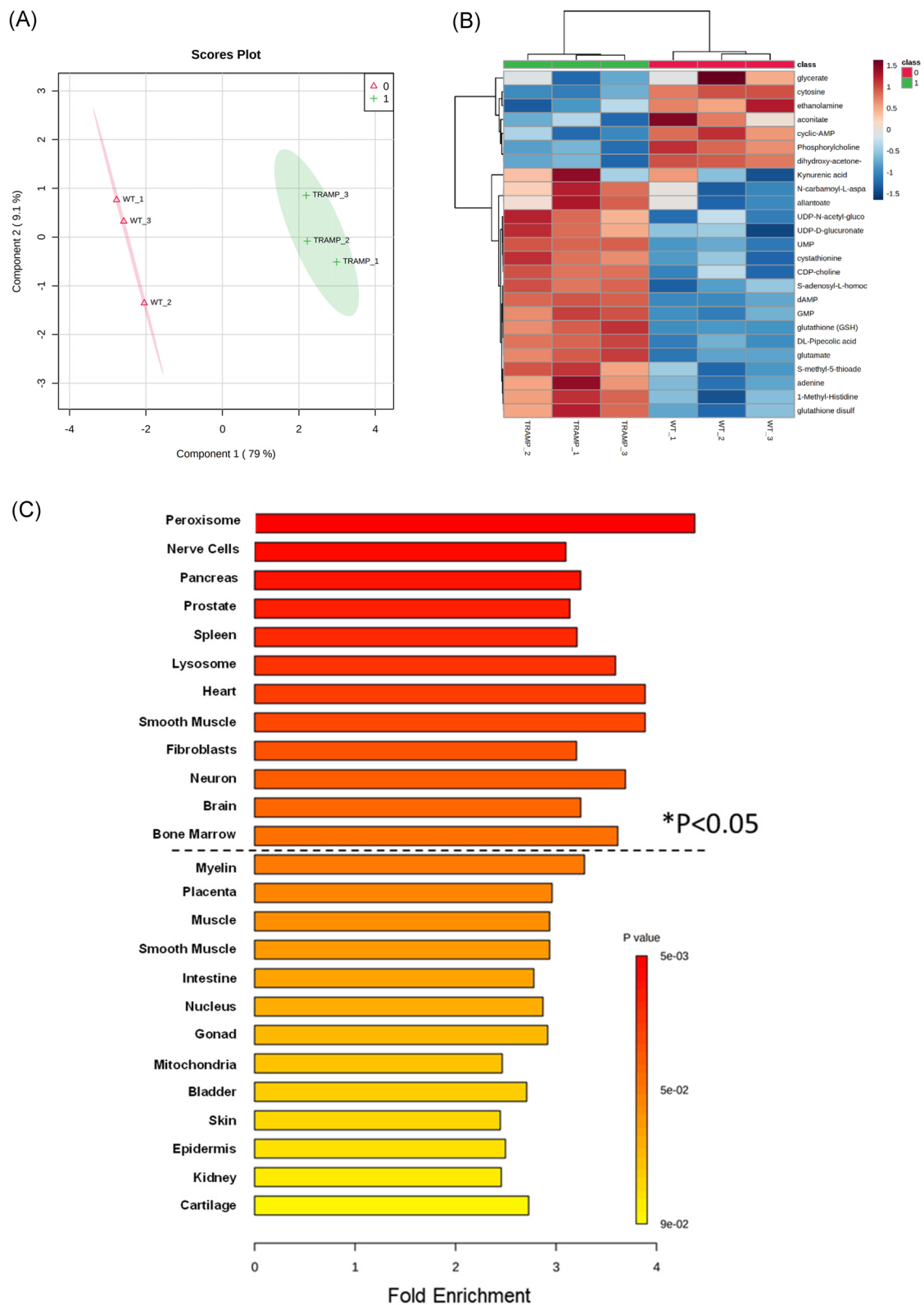


FIGURE 3 Metabolomic analyses of TRAMP NECa model using MetaboAnalyst 4.0. (A) Metabolic profile of TRAMP and wild type (WT) mouse prostates visualized by supervised partial least-squares discriminant analysis clustered by the samples with the three biological replicates of WT (red triangle) and three biological replicates of TRAMP NECa (green cross). (B) Heatmap for relative abundances of top 25 metabolites in WT prostate and TRAMP NECa matched pairs (i.e., WT1 vs. TRAMP1, WT2 vs. TRAMP2, and WT3 vs. TRAMP3). Columns represent each biological replicate, and rows represent individual metabolites. The more abundant metabolites in TRAMP appeared red, and the less metabolites were colored blue. (C) Location-based metabolite sets enrichment analysis (MSEA). The dashed lines indicate the cutoff p -value ($*p < 0.05$). The color of the scale bar represents the p value [Color figure can be viewed at wileyonlinelibrary.com]

de novo phospholipid syntheses in the aggressively growing NECa (Figure 4).

Many cancers prefer the less efficient but faster aerobic glycolysis (Warburg effect) to generate energy by converting glucose to lactate to support cancer cell growth and proliferation under hypoxic TME, while the differentiated normal cells mainly rely on efficient but slow mitochondrial oxidative phosphorylation to maintain cellular energetics.³⁵ In previous collaborative work, we have shown that an increase in aerobic glycolysis in the *Pten-TP53* double deficient prostate cancer cells through a specific elevation of hexokinase-2 (HK-2) isoform, but *Pten-KO* alone had minimal impact on HK-2 expression or glycolysis.³⁶ In our current metabolomic analysis, we found that the intermediate metabolites of *glycolysis* and *pyruvate metabolisms*, including oxaloacetate and dihydroxyacetone phosphate, were modestly decreased in the *Pten-KO* prostate (Figure 2; Table S1), therefore, not supporting increased glycolytic energy metabolism. Rather the metabolomics outcome implicated an overall reshunting of glucose to pentose phosphate cycle to sustain the generation of NADPH for GSH/GSSG redox, pentose moieties for purine and pyrimidine nucleotides, and to glucuronidation Phase II detoxification activities. The TRAMP NECa shared similar down-regulation of glycolysis-citrate cycle metabolism (Figure 4), in spite of the onco-driver differences from the *Pten-KO* model.

4.1 | Limitations

The major caveat for the employed metabolome platform was a bias for hydrophilic metabolites, excluding almost all lipids, fatty acids, and sterols and their hydrophobic metabolites. Another weakness was the lack of anatomical (different prostate lobes) and cell-type distribution information of the metabolites due to the homogenization of each tissue sample. Future efforts should include lipidomics for the hydrophobic metabolites, as well as imaging MS approaches that provide metabolite mapping resolution to cellular or subcellular organelle level on tissue microscopic slice.

5 | CONCLUSIONS

In spite of the limitations of the extraction and analytical platform, the aqueous metabolomic change patterns in *Pten-KO* prostate suggested a significant reshunting of glucose metabolism, GSH synthesis, and redox and arginine to ornithine catabolism for increased proliferation of transformed epithelial cells and immunosuppression. The *Pten-KO* model exhibited some unique shared metabolism signature with human prostate cancer such as cholesterol sulfate that was decreased in the TRAMP model. While sharing similarities in greater pools of cystathionine and GSH/GSSG redox pair, and of ribosyl and deoxyribosyl nucleotides for nucleic acid syntheses, the TRAMP model stood out in the elevated pools of amino acids for protein synthesis and methylation epigenetic regulations, plus a likelihood of increased de novo synthesis of phospholipids. The

metabolomics datasets from these two experimental models of prostate carcinogenesis are accessible to readers for data mining and interpretation.

ACKNOWLEDGMENTS

The authors thank Dr. Christopher J. Kemp and Mr. Kay Gurley at the Fred Hutchinson Cancer Research Center for supplying the frozen bio-specimens; Dr. Su-Ni Tang at Texas Tech University Health Sciences Center for help on tissue processing. This study has been supported, in part, by R01CA172169 grant (to J. L.) and R21CA218774 grant (to J. L.) from US National Cancer Institute and Penn State College of Medicine Start-up fund (to J. L.).

CONFLICT OF INTEREST

The authors declare that there are no conflict of interest.

DATA AVAILABILITY STATEMENT

Data that supports the findings of this study are available in the supplementary materials of this article.

REFERENCES

- Feng J, Zhang Q, Zhou Y, et al. Integration of proteomics and metabolomics revealed metabolite-protein networks in ACTH-secreting pituitary adenoma. *Front Endocrinol (Lausanne)*. 2018;9:678.
- Hanahan D, Weinberg RA. Hallmarks of cancer: the next generation. *Cell*. 2011;144(5):646-674.
- Geybels MS, Fang M, Wright JL, et al. PTEN loss is associated with prostate cancer recurrence and alterations in tumor DNA methylation profiles. *Oncotarget*. 2017;8(48):84338-84348.
- Han B, Mehra R, Lonigro RJ, et al. Fluorescence in situ hybridization study shows association of PTEN deletion with ERG rearrangement during prostate cancer progression. *Mod Pathol*. 2009;22(8):1083-1093.
- Yoshimoto M, Cutz JC, Nuin PA, et al. Interphase FISH analysis of PTEN in histologic sections shows genomic deletions in 68% of primary prostate cancer and 23% of high-grade prostatic intra-epithelial neoplasias. *Cancer Genet Cytogenet*. 2006;169(2):128-137.
- Song MS, Salmena L, Pandolfi PP. The functions and regulation of the PTEN tumour suppressor. *Nat Rev Mol Cell Biol*. 2012;13(5):283-296.
- Gómez-Cebrián N, Rojas-Benedicto A, Albors-Vaquero A, López-Guerrero JA, Pineda-Lucena A, Puchades-Carrasco L. Metabolomics Contributions to the discovery of prostate cancer biomarkers. *Metabolites*. 2019;9(3).
- Wang S, Gao J, Lei Q, et al. Prostate-specific deletion of the murine *Pten* tumor suppressor gene leads to metastatic prostate cancer. *Cancer Cell*. 2003;4(3):209-221.
- García AJ, Ruscetti M, Arenzana TL, et al. *Pten* null prostate epithelium promotes localized myeloid-derived suppressor cell expansion and immune suppression during tumor initiation and progression. *Mol Cell Biol*. 2014;34(11):2017-2028.
- Zhang J, Kim S, Li L, Kemp CJ, Jiang C, Lü J. Proteomic and transcriptomic profiling of *Pten* gene-knockout mouse model of prostate cancer. *Prostate*. 2020;80(7):588-605.
- Chiaverotti T, Couto SS, Donjacour A, et al. Dissociation of epithelial and neuroendocrine carcinoma lineages in the transgenic adenocarcinoma of mouse prostate model of prostate cancer. *Am J Pathol*. 2008;172(1):236-246.
- Wang L, Zhang J, Zhang Y, et al. Lobe-specific lineages of carcinogenesis in the transgenic adenocarcinoma of mouse prostate and

- their responses to chemopreventive selenium. *Prostate*. 2011; 71(13):1429-1440.
13. Yuan M, Breitkopf SB, Yang X, Asara JM. A positive/negative ion-switching, targeted mass spectrometry-based metabolomics platform for bodily fluids, cells, and fresh and fixed tissue. *Nat Protoc*. 2012;7(5):872-881.
 14. Xia J, Sinelnikov IV, Han B, Wishart DS. MetaboAnalyst 3.0—making metabolomics more meaningful. *Nucleic Acids Res*. 2015;43(W1):W251-W257. doi:10.1093/nar/gkv380
 15. Deus CM, Yambire KF, Oliveira PJ, Raimundo N. Mitochondria-Lysosome crosstalk: from physiology to neurodegeneration. *Trends Mol Med*. 2020;26(1):71-88.
 16. Zabala-Letona A, Arruabarrena-Aristorena A, Martín-Martín N, et al. mTORC1-dependent AMD1 regulation sustains polyamine metabolism in prostate cancer. *Nature*. 2017;547(7661):109-113.
 17. Jung K, Reszka R, Kamlage B, et al. Tissue metabolite profiling identifies differentiating and prognostic biomarkers for prostate carcinoma. *Int J Cancer*. 2013;133(12):2914-2924.
 18. Ren S, Shao Y, Zhao X, et al. Integration of metabolomics and transcriptomics reveals major metabolic pathways and potential biomarker involved in prostate cancer. *Mol Cell Proteomics*. 2016; 15(1):154-163.
 19. Lu W, Su X, Klein MS, Lewis IA, Fiehn O, Rabinowitz JD. Metabolite measurement: pitfalls to avoid and practices to follow. *Annu Rev Biochem*. 2017;86:277-304.
 20. Teichert F, Verschoyle RD, Greaves P, et al. Metabolic profiling of transgenic adenocarcinoma of mouse prostate (TRAMP) tissue by ¹H-NMR analysis: evidence for unusual phospholipid metabolism. *Prostate*. 2008;68(10):1035-1047.
 21. Morey Kinney SR, Smiraglia DJ, James SR, Moser MT, Foster BA, Karpf AR. Stage-specific alterations of DNA methyltransferase expression, DNA hypermethylation, and DNA hypomethylation during prostate cancer progression in the transgenic adenocarcinoma of mouse prostate model. *Mol Cancer Res*. 2008;6(8): 1365-1374.
 22. Phin S, Moore MW, Cotter PD. Genomic rearrangements of PTEN in prostate cancer. *Front Oncol*. 2013;3:240.
 23. Kelly RS, Sinnott JA, Rider JR, et al. The role of tumor metabolism as a driver of prostate cancer progression and lethal disease: results from a nested case-control study. *Cancer Metab*. 2016;4: 22.
 24. Mossman D, Park S, Hall MN. mTOR signalling and cellular metabolism are mutual determinants in cancer. *Nat Rev Cancer*. 2018; 18(12):744-757.
 25. Jerjees DA, Negm OH, Alabdullah ML, et al. The mammalian target of rapamycin complex 1 (mTORC1) in breast cancer: the impact of oestrogen receptor and HER2 pathways. *Breast Cancer Res Treat*. 2015;150(1):91-103.
 26. Mathur D, Stratikopoulos E, Ozturk S, et al. PTEN Regulates glutamine flux to pyrimidine synthesis and sensitivity to dihydroorotate dehydrogenase inhibition. *Cancer Discov*. 2017;7(4):380-390.
 27. Bansal A, Simon MC. Glutathione metabolism in cancer progression and treatment resistance. *J Cell Biol*. 2018;217(7):2291-2298.
 28. Stabler S, Koyama T, Zhao Z, et al. Serum methionine metabolites are risk factors for metastatic prostate cancer progression. *PLoS One*. 2011;6(8):e22486.
 29. Belalcázar AD, Ball JG, Frost LM, Valentovic MA, Wilkinson J. Transsulfuration is a significant source of sulfur for glutathione production in human mammary epithelial cells. *ISRN Biochem*. 2013; 637897. doi:10.1155/2013/637897
 30. Shuvalov O, Petukhov A, Daks A, Fedorova O, Vasileva E, Barlev NA. One-carbon metabolism and nucleotide biosynthesis as attractive targets for anticancer therapy. *Oncotarget*. 2017;8(14):23955-23977.
 31. Li Y, He L, Zeng N, et al. Phosphatase and tensin homolog deleted on chromosome 10 (PTEN) signaling regulates mitochondrial biogenesis and respiration via estrogen-related receptor alpha (ERRalpha). *J Biol Chem*. 2013;288(35):25007-25024.
 32. Yue S, Li J, Lee SY, et al. Cholesteryl ester accumulation induced by PTEN loss and PI3K/AKT activation underlies human prostate cancer aggressiveness. *Cell Metab*. 2014;19(3):393-406.
 33. Eberlin LS, Dill AL, Costa AB, et al. Cholesterol sulfate imaging in human prostate cancer tissue by desorption electrospray ionization mass spectrometry. *Anal Chem*. 2010;82(9):3430-3434.
 34. Chen CY, Chen J, He L, Stiles BL. PTEN: Tumor suppressor and metabolic regulator. *Front Endocrinol (Lausanne)*. 2018;9:338.
 35. Zhou X, Yang X, Sun X, et al. Effect of PTEN loss on metabolic reprogramming in prostate cancer cells. *Oncol Lett*. 2019;17(3):2856-2866.
 36. Wang L, Xiong H, Wu F, et al. Hexokinase 2-mediated Warburg effect is required for PTEN- and p53-deficiency-driven prostate cancer growth. *Cell Rep*. 2014;8(5):1461-1474.

SUPPORTING INFORMATION

Additional supporting information may be found in the online version of the article at the publisher's website.

How to cite this article: Kim S, Li L, Zhang J, Jiang C, Lü J. Aqueous metabolome of tissue-specific conditional *Pten*-knockout mouse prostate cancer and TRAMP neuroendocrine carcinoma. *The Prostate*. 2022;82:154-166. <https://doi.org/10.1002/pros.24256>